Quantum Transport of Rydberg Excitons with Synthetic Spin-Exchange Interactions

Fan Yang,[1] Shuo Yang,[1,*] and Li You[1,2,†]

[1]*State Key Laboratory of Low Dimensional Quantum Physics, Department of Physics,*
Tsinghua University, Beijing 100084, China
[2]*Beijing Academy of Quantum Information Sciences, Beijing 100193, China*

We present a scheme for engineering quantum transport dynamics of spin excitations in a chain of laser-dressed Rydberg atoms, mediated by synthetic spin exchange arising from diagonal van der Waals interaction. The dynamic tunability and long-range interaction feature of our scheme allows for the exploration of transport physics unattainable in conventional spin systems. As two concrete examples, we first demonstrate a topological exciton pumping protocol that facilitates quantized entanglement transfer, and second we discuss a highly nonlocal correlated transport phenomenon which persists even in the presence of dephasing. Unlike previous schemes, our proposal requires neither resonant dipole-dipole interaction nor off-diagonal van der Waals interaction. It can be readily implemented in existing experimental systems.

Developing controlled large-scale quantum systems constitutes a central goal of quantum simulation and quantum computation [1,2]. Among the variety of physical realizations, neutral atoms present several unique advantages [3], such as their inherent qubit identity, long coherence time, flexible state maneuverability, as well as tunable qubit-qubit interactions, for instance, mediated by Rydberg states [4]. The continued progress in Rydberg-atom studies offers great potential for probing many-body dynamics [5–9]. With improved operation fidelity [10] and increased system size [11], quantum simulation on the Rydberg atom based platform [8,12] is becoming increasingly attractive.

The transport of a particle or spin via quantum state-changing interactions is essential for understanding energy or information flow. Emulating such problems on a quantum simulator constitutes a focused thrust within the broad quantum physics community [13–17]. Earlier efforts based on Rydberg-atom systems have provided first insights [18–24], where transport of spin excitation is facilitated typically by resonant dipole-dipole interaction (DDI) or by off-diagonal van der Waals (vdW) flip-flop interaction between Rydberg states. They include direct spin-exchange between different Rydberg states [18–20], second-order exchange between the ground state and the Rydberg state [21–23], and a fourth-order process inside ground internal state manifolds [24–26].

In this Letter, we propose a simpler yet as effective method for engineering exciton transport dynamics in a Rydberg-atom system. The use of resonant DDI or flip-flop vdW interaction is avoided. Instead, our main idea relies on a perturbative spin-exchange process by off-resonantly dressing the ground state to a Rydberg state. Capitalizing on the diagonal vdW interaction-induced Rydberg level shift, perturbations from different pathways collectively contribute to a net exchange interaction between the ground and the Rydberg states. When exciton-exciton interaction as well as dephasing are included, our model system is shown to be capable of simulating various transport dynamics unattainable in conventional spin systems. In the first example, we establish an interesting topological pumping protocol, whereby the exciton experiences a quantized center-of-mass motion. In the second example, we show that the long-range interaction between excitons permits the formation of high-order magnon bound state, which exhibits nonlocal correlations even when ballistic transport turns into classical diffusion due to dephasing.

Model.—The system we study is an array of individually trapped cold atoms, dressed by laser fields that couple the ground state $|g\rangle$ to a Rydberg state $|r\rangle$ [7,10]. It is modeled by the Hamiltonian

$$\hat{H} = \sum_i \frac{\Omega_i}{2}\hat{\sigma}_x^i + \sum_i \Delta_i \hat{\sigma}_{rr}^i + \sum_{i<j} V(\mathbf{r}_{ij})\hat{\sigma}_{rr}^i \hat{\sigma}_{rr}^j, \quad (1)$$

where Ω_i and Δ_i are Rabi frequencies and detunings of the dressing field [Fig. 1(a)], $\hat{\sigma}_x^i = |r_i\rangle\langle g_i| + |g_i\rangle\langle r_i|$ and $\hat{\sigma}_{\alpha\alpha}^i = |\alpha_i\rangle\langle\alpha_i|$ ($\alpha = g, r$) are spin-flip and projection operators for the ith atom (located at $\mathbf{r}_i$), and $V(\mathbf{r}_{ij}) = C_6/|\mathbf{r}_i - \mathbf{r}_j|^6$ is the diagonal vdW interaction between atoms in the Rydberg state [6] (we take $C_6 > 0$).

First, we consider the dynamics of a single Rydberg exciton. In the limit of large detuning with $\Omega_i \ll |\Delta_i|$, $|\Delta_i + V(\mathbf{r}_{ij})|$, and $|\Delta_i - \Delta_j| \ll |\Delta_{i/j}|$, the singly excited state set $\{|\Psi_i\rangle = |g_1 g_2 \cdots r_i \cdots g_N\rangle, i = 1, 2, \ldots, N\}$ forms
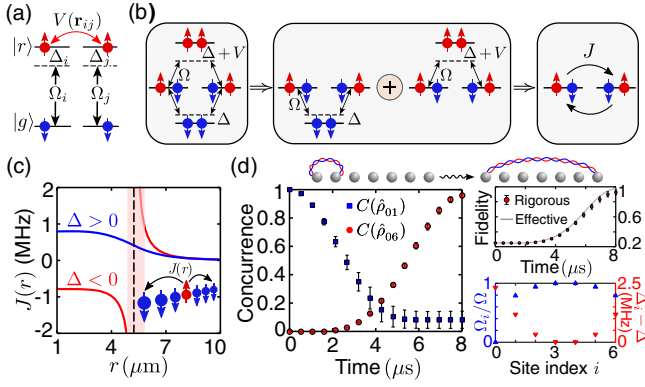
FIG. 1. (a) Level structure for the proposed atomic system. We consider ^{87}Rb atom with $|g\rangle = |5S_{1/2}, F = 2, m_F = -2\rangle$, $|r\rangle = |70S, J = 1/2, m_J = -1/2\rangle$ [10]. (b) Illustration of the mechanism for generating a synthetic spin-exchange interaction. (c) Synthetic exchange strength $J(r)$ vs distance r for $\Omega/2\pi = 5$ and $\Delta/2\pi = \pm 50$ MHz. The dashed lines denote the facilitation condition $\Delta + V(r) = 0$. (d) The left panel shows the concurrence for the first two nodes $[C(\hat{\rho}_{01})]$ and the two end nodes $[C(\hat{\rho}_{06})]$. The right panel shows the fidelity to the target state $(|r_0 g_1 \cdots g_6\rangle - i|g_0 g_1 \cdots r_6\rangle)/\sqrt{2}$ (upper figure, the rigorous and effective results are obtained with $\hat{H}$ and $\hat{H}_{\text{eff}}$, respectively) and values of dressing parameters (lower figure) with $V(d) = 3\Delta$ ($\Delta > 0$) and $d = 4.4$ μm. The numerical data represent averages over 500 calculations, assuming a Gaussian distribution of atomic position along the chain direction with 0.1 μm standard deviation. The error bars mark 1 standard deviation intervals.

a quasidegenerate subspace Π_1. As a result, the perturbative coupling with the rest of the Hilbert space can induce strong state mixing inside Π_1, giving rise to coherent position exchanges of the exciton. To clarify the basic physics, we take the example of $N = 2$. As shown in Fig. 1(b), the degenerate states $|r_1 g_2\rangle$ and $|g_1 r_2\rangle$ are off-resonantly coupled to $|g_1 g_2\rangle$ and $|r_1 r_2\rangle$, which can be approximately treated as two Raman pathways. For the noninteracting case ($V = 0$), the contributions of these two paths cancel out. In the presence of the vdW interaction, the level shift V for $|rr\rangle$ causes the two pathways collectively to yield a nonvanishing spin exchange interaction $J = \Omega^2/4\Delta - \Omega^2/4(\Delta + V)$. For a many-body system, applying second-order Van Vleck perturbation theory [27] to the original model [Eq. (1)] and dropping the constant $-\sum_j \Omega_j^2/4\Delta_j$, we arrive at an effective Hamiltonian [28],

$$\hat{H}_{\text{eff}} = \sum_i \left(\Delta_i + \frac{\Omega_i^2}{2\Delta_i}\right)\hat{\sigma}_{rr}^i + \sum_{i \neq j} I_{ij}\hat{\sigma}_{rr}^i\hat{\sigma}_{gg}^j + J_{ij}\hat{\sigma}_+^i\hat{\sigma}_-^j, \quad (2)$$

where $\hat{\sigma}_+^i = |r_i\rangle\langle g_i|$ and $\hat{\sigma}_-^i = |g_i\rangle\langle r_i|$ are spin raising and lowering operators for the ith atom. The Ising-type interaction I_{ij} and the spin-exchange interaction J_{ij}, respectively, take the following forms

$$I_{ij} = \frac{\Omega_j^2 V(\mathbf{r}_{ij})}{4\Delta_j[\Delta_j + V(\mathbf{r}_{ij})]}, \qquad J_{ij} = \sum_{\beta=i,j}\frac{\Omega_i\Omega_j V(\mathbf{r}_{ij})}{8\Delta_\beta[\Delta_\beta + V(\mathbf{r}_{ij})]}.$$

In contrast to earlier dressing schemes [25,26], the spin-exchange interaction we find constitutes a pure synthetic interaction as the initial Hamiltonian Eq. (1) contains only diagonal vdW interactions. It exhibits different r dependence compared with previous schemes [Fig. 1(c)] and is highly tunable in terms of Ω_i and Δ_i. This effective model is not restricted to any particular type of lattice, and this work considers the simplest one-dimensional periodic chain with a spacing d.

The exciton transport is conveniently described by mapping spins to hard-core bosons with $\hat{\sigma}_+^i = \hat{a}_i^\dagger$ and $\hat{\sigma}_-^i = \hat{a}_i$, where $\hat{a}_i^\dagger$ ($\hat{a}_i$) creates (annihilates) a Rydberg exciton at site i. The effective Hamiltonian for a single exciton can then be expressed in a tight-binding form with $\hat{H}_{\text{eff}} = \sum_i \mu_i \hat{a}_i^\dagger \hat{a}_i + \sum_{i<j} J_{ij}(\hat{a}_i^\dagger \hat{a}_j + \hat{a}_j^\dagger \hat{a}_i)$, where $\mu_i = \Delta_i + \Omega_i^2/2\Delta_i + \sum_{j \neq i} I_{ij}$ is the on-site potential. To benchmark the effective model, we focus on an entanglement distribution protocol, in which the entangled state $(|r_0 g_1\rangle + |g_0 r_1\rangle)/\sqrt{2}$ is transferred to $(|r_0 g_N\rangle + e^{i\phi}|g_0 r_N\rangle)/\sqrt{2}$ over a chain of $N + 1$ atoms. For systems dominated by nearest-neighbor (NN) hopping, perfect entanglement transfer can be achieved when the conditions $\mu_i = \mu$, $J_{i,i+1} = J\sqrt{i(N-i)}$ [29] are satisfied. The initial entangled state can be set up via Rydberg blockade, and the perfect transfer condition can be met by tuning local parameters Ω_i and Δ_i. As verified by numerical results ($N = 6$) shown in Fig. 1(d), entanglement between the two end nodes gradually establishes and approaches the maximal value eventually, calibrated by their concurrence [30] and state fidelity. The potential existence of disorder in atomic positions is also taken into account in the calculation [7]. As long as the disorder-induced interaction fluctuation δV_{ij} is much smaller than V_{ij} itself ($\delta V_{ij} \ll V_{ij}$), the transport efficiency remains high [28]. We note that all numerical results presented in this work are based on solving the exact model Eq. (1).

In addition to simulating coherent dynamics, the system we consider also provides a platform for probing the crossover between coherent and incoherent transport. In the presence of dephasing [31,32], the evolution of the density matrix $\hat{\rho}$ is governed by the master equation $\partial_t\hat{\rho} = -i[\hat{H}, \hat{\rho}] + \sum_i \mathcal{L}[\sqrt{\gamma}\hat{\sigma}_{rr}^i]\hat{\rho}$, where the Lindblad operator $\mathcal{L}$ gives $\mathcal{L}[\hat{\sigma}]\hat{\rho} = \hat{\sigma}\hat{\rho}\hat{\sigma}^\dagger - \frac{1}{2}(\hat{\sigma}^\dagger\hat{\sigma}\hat{\rho} + \hat{\rho}\hat{\sigma}^\dagger\hat{\sigma})$. For weak dephasing ($\gamma \ll |\Delta_i|$), the dynamics remain confined within the subspace Π_1 for times smaller than $t_c = \min\{\Delta_i^2/\gamma\Omega_i^2\}$, while for $t > t_c$ incoherent spin flips and exciton growth takes over [31]. In the transport regime ($t < t_c$), the dynamics can be effectively described by $\partial_t\hat{\rho} = -i[\hat{H}_{\text{eff}}, \hat{\rho}] + \sum_i \mathcal{L}[\sqrt{\gamma}\hat{a}_i^\dagger\hat{a}_i]\hat{\rho}$, equivalent to the Haken-Reineker-Strobl

(HRS) model with coherent hopping and on-site dephasing [33–35]. The exciton motion remains coherent for $t < 1/\gamma$, and exhibits incoherent features as it enters the diffusion region $t > 1/\gamma$ [28].

Next we discuss the case involving multi-excitons. With n Rydberg excitons, the quasidegenerate perturbation analysis can no longer be simply applied to the subspace Π_n spanned by the states $\{|\Psi_{i_1,\ldots,i_n}\rangle = |g_1 \cdots r_{i_1} \cdots r_{i_n} \cdots g_N\rangle, i_1 < \cdots < i_n\}$, since the large vdW interaction between excitons removes some of the degeneracy. For example, in the $n = 2$ case, the doubly excited subspace Π_2 can be decomposed into $\Pi_2 = \Pi_2' \bigcup \Pi_2''$, with Π_2' spanned by the dimer states $\{|\Psi_{i,i+1}\rangle = |g_1 \cdots r_i r_{i+1} \cdots g_N\rangle, i = 1,\ldots,N\}$ and Π_2'' the complementary set of Π_2'. If $V(\mathbf{r}_{i,i+1})$ is of the same order as $|\Delta_i|$, Π_2' and Π_2'' forms two decoupled quasidegenerate subspaces. Inside Π_2', the dimer states are coupled to each other through next-nearest-neighbor (NNN) hoppings $\sum_i J_i^{(2)} \hat{\sigma}_+^i \hat{\sigma}_{rr}^{i+1} \hat{\sigma}_-^{i+2} + \text{H.c.}$, with an effective three-body exchange interaction

$$J_i^{(2)} \approx \frac{\Omega_i \Omega_{i+2} V(\mathbf{r}_{i,i+2})}{4[\Delta_i + V(\mathbf{r}_{i,i+1})][\Delta_i + V(\mathbf{r}_{i,i+1}) + V(\mathbf{r}_{i,i+2})]}.$$

For exciton dynamics inside Π_2'', the perturbation analysis yields an effective Hamiltonian $\hat{H}_{\text{eff}}' = \hat{H}_{\text{eff}} + \hat{H}_{\text{int}}$ [28], where $\hat{H}_{\text{eff}}$ is the single-exciton effective Hamiltonian, while $\hat{H}_{\text{int}} = \sum_{i<j} U_{ij} \hat{a}_i^\dagger \hat{a}_j^\dagger \hat{a}_j \hat{a}_i$ describes exciton-exciton interactions, with strength $U_{ij} = V(\mathbf{r}_{ij}) - 2(I_{ij} + I_{ji})$. For the case of n excitons, the dynamics of the system can still be approximately described by $\hat{H}_{\text{eff}}'$, as long as the initial separations between excitons are large enough to ensure that their mutual interactions are much smaller than the detuning. If some of the excitons are close to each other initially, they will form a tightly bound state (such as the dimer state described above), whose transport property needs further elaborations.

When simulating transport physics, we focus on the case where the total exciton number $\hat{N}_e = \sum_i \hat{\sigma}_{rr}^i = \sum_i \hat{a}_i^\dagger \hat{a}_i$ is conserved. However, $\hat{N}_e$ is not strictly conserved due to a finite spin-flip probability $|\Omega_i/\Delta_i|^2$ for each (ith) atom. This could significantly influence the quality of our simulations especially as the number of atoms increases. However, for observables whose expectation values only depend on the diagonal elements of $\hat{\rho}$ (e.g., density correlations), the simulation results can be refined via postselection based on projective measurements. If the dynamics of n excitons are of interest, the expectation values of the observables are calculated by the refined density matrix $\hat{\rho}_p = p^{-1} \sum_k p_k \hat{P}_k$, where $\hat{P}_k = |\phi_k\rangle\langle\phi_k|$ denotes the projection operator of state $|\phi_k\rangle \in \Pi_n$, and $p_k = \text{Tr}(\hat{\rho}\hat{P}_k)$ is the probability of the measurement. The postselection probability $p = \sum_k p_k$ scales as $1 - N\Omega^2/2\Delta^2$,

which is acceptable for a reasonable sized system ($p \approx 0.75$ for $\Delta/\Omega = 10$ and $N = 50$).

Example 1.—To illustrate the dynamical tunability of our scheme, we consider an implementation for topological exciton pumping, for which a time-dependent and site-dependent exchange interaction is required [36–41]. A periodic system with broken parity symmetry is assumed [42], with three lattice sites (labeled as A, B, C, and separated by d) forming a unit cell (with the period $l = 3d$), dressed by control fields of three intensities [Fig. 2(a)] with corresponding Rabi frequencies $\Omega_A, \Omega_B, \Omega_C = \Omega \times \{\sin^2(\phi + \pi/4), \sin^2(\phi), \sin^2(\phi - \pi/4)\}$ and ϕ a time-dependent control parameter. Such a dressing scheme can be realized by using three independently controlled acousto-optic deflectors. Retaining the NN interaction, the system can be described by the generalized Rice-Mele Hamiltonian [43]

$$\hat{H}_{\text{eff}} = \sum_i (J_A \hat{a}_i^\dagger \hat{b}_i + J_B \hat{b}_i^\dagger \hat{c}_i + J_C \hat{c}_i^\dagger \hat{a}_{i+1} + \text{H.c.})$$
$$+ \sum_i (\mu_A \hat{a}_i^\dagger \hat{a}_i + \mu_B \hat{b}_i^\dagger \hat{b}_i + \mu_C \hat{c}_i^\dagger \hat{c}_i), \quad (3)$$

where $\hat{a}_i$, $\hat{b}_i$, and $\hat{c}_i$ are exciton annihilation operators for site A, B, and C of the ith unit, respectively. According to the Bloch theorem, this system can be described in the quasimomentum k space with a single-particle Hamiltonian $\hat{\mathcal{H}}(k,\phi)$ [28], which is also periodic in ϕ. Thus, we can define the energy band in the synthetic space $\mathbf{k} = (k, \phi)$ with the first Brillouin zone (BZ) $k \in (-\pi/l, \pi/l]$ and $\phi \in (-\pi/2, \pi/2]$. The topology of each band is characterized by the Chern number
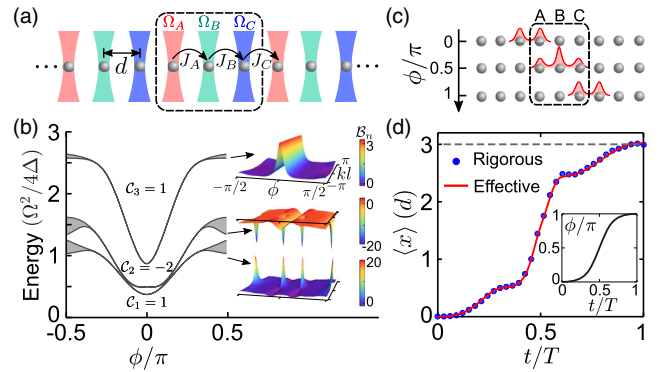

FIG. 2. (a) Illustration of the dressing scheme for topological exciton pumping. (b) Energy band and Berry curvature of the effective model. (c) Illustration of the pumping sequence. (d) Mean displacement $\langle x \rangle$ of the exciton at different time t. The blue dots are calculated by the refined density matrix using the exact model Eq. (1), and the red lines are obtained with the effective Hamiltonian Eq. (3). The inset shows the modulation detail $\phi/\pi = \frac{1}{2} + \{(\tanh[5.6(t/T - 1/2)])/2\tanh(2.8)\}$. The simulations are performed with $\Omega/2\pi = 5$ MHz, $\Delta/2\pi = 20$ MHz, $V(d) = 3\Delta$, $N = 12$, and $T = 27.7$ μs.

$$C_n = \frac{1}{2\pi} \int_{BZ} \mathcal{B}_n(\mathbf{k}) d^2\mathbf{k}, \tag{4}$$

where $\mathcal{B}_n(\mathbf{k}) = i(\langle \partial_\phi u_n | \partial_k u_n \rangle - \text{c.c.})$ is the Berry curvature of the nth band, and $|u_n\rangle$ is the eigenstate of $\hat{\mathcal{H}}(k, \phi)$. For the system considered above, we find three gapped bands with respective nontrivial topological numbers $\mathcal{C}_1, \mathcal{C}_2, \mathcal{C}_3 = \{1, -2, 1\}$, as shown in Fig. 2(b).

In this case, we can implement Thouless pumping [36], while the parameter $\phi(t)$ is slowly modulated in time t. After a pumping cycle in which ϕ changes by π, the Hamiltonian returns to its initial form. If an energy band is filled or homogeneously populated, the mean displacement $\langle x \rangle$ of the exciton after one pumping cycle is quantized in units of lattice constant, i.e., $\langle x \rangle / l = \mathcal{C}_n$. For our system, the energy gap $\Omega^2 V(d)/8\Delta[\Delta + V(d)]$ between the upper and the middle band is about 2 orders of magnitude larger than the gap between the middle and the lower band. Thus, to achieve better adiabaticity, we consider motion of the exciton within the upper band. As indicated by the pumping sequence shown in Fig. 2(c), we first shine a resonant field on sites C_j and A_{j+1} to produce an entangled state $|\psi_j\rangle = (1/\sqrt{2})(\hat{c}_j^\dagger + \hat{a}_{j+1}^\dagger)|0\rangle$ using Rydberg blockade. With such an initialization and $\phi(0) = 0$, we create an equally weighted Bloch state for the upper band. Then, we adiabatically ramp ϕ from 0 to π, and observe the position of the exciton. As shown in Fig. 2(d), the mean displacement of the exciton after one pumping cycle is indeed $\langle x \rangle \approx 3d = l$, in agreement with the topology of the upper band. Since this energy band is almost flat in the k dimension, such a quantized motion indicates a high-efficiency entangled state transfer from $|\psi_j\rangle$ to $|\psi_{j+1}\rangle$. It is worth pointing out that during the long pumping cycle T, the NNN interaction also comes into play. In fact, the long-range interaction induced NNN hoppings $\sum_i (J_A' \hat{a}_i^\dagger \hat{c}_i + J_B' \hat{b}_i^\dagger \hat{a}_{i+1} + J_C' \hat{c}_i^\dagger \hat{b}_{i+1} + \text{H.c.})$ and the modifications to on-site potential can be viewed as perturbations to $\hat{H}_{\text{eff}}$. We find that although these perturbations can significantly modify the spread $\langle x^2 \rangle$ of the exciton, they do not change the mean displacement $\langle x \rangle$ [28]. Such a robust center-of-mass (c.m.) motion is protected by the topology of the band, which is invariant under continuous deformation of the Hamiltonian [44,45].

Example 2.—The strong and nonlocal exciton-exciton interaction in the proposed system also makes it feasible for studying correlated transport [46,47]. Here, we consider the dynamics of two excitons in a homogeneously dressed $(\Delta_i = \Delta$ and $\Omega_i = \Omega)$ chain with $V(2d) \ll |\Delta|$.

We first consider the dynamics of the dimer state $|\Psi_{i,i+1}\rangle$, which can be prepared via antiblockade excitation satisfying $2\Delta + V(d) = 0$ [48]. As explained previously, such a tightly bound state can migrate through NNN hopping [see the upper panel of Fig. 3(a)], the hopping rate of which can be significant near the facilitation [7]
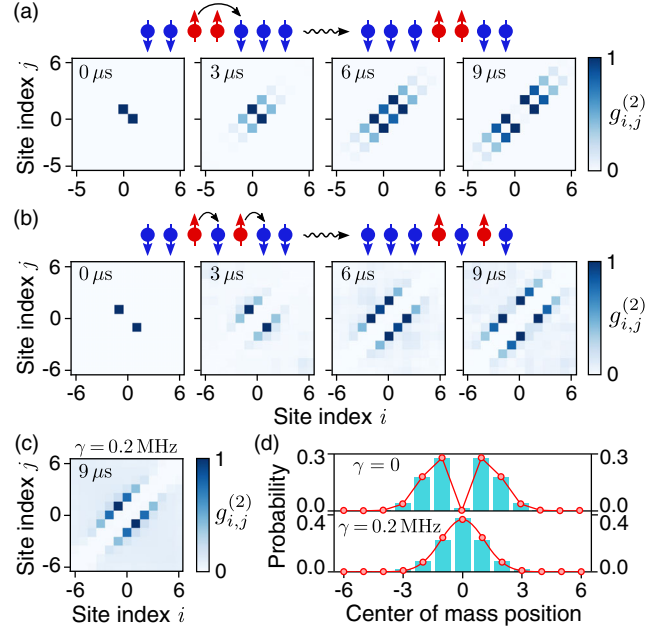

FIG. 3. (a) Evolution of the density-density correlation $g_{i,j}^{(2)}$ for the dimer state $|\Psi_{i,i+1}\rangle$. (b) Evolution of the density-density correlation for the high-order bound state $|\Psi_{i,i+2}\rangle$. (c) Correlation function at 9 μs, with the same initial state in (b) and $\gamma = 0.2$ MHz. (d) Normalized probability distribution of the c.m. position. The blue bars are numerical results obtained from the exact model with projective measurement, and the red dotted lines are fitted curves using a Bessel function of the first kind (upper) and a Gaussian function (lower), respectively. The parameters used are $\Omega/2\pi = 5$ MHz, $\Delta/2\pi = -400$ MHz, $V(d) = -1.1\Delta$, $N = 12$ in (a), and $\Delta/2\pi = 30$ MHz, $V(d) = 3\Delta$, $N = 13$ in (b)–(d). The correlation functions are normalized to the maximal value.

region $\Delta + V(d) = 0$. This correlated transport can be measured by the second-order correlation function $g_{i,j}^{(2)} = \langle \hat{a}_i^\dagger \hat{a}_j^\dagger \hat{a}_j \hat{a}_i \rangle$. As shown in Fig. 3(a), we find $g_{i,j}^{(2)}$ rapidly spreads on the diagonals $j = i \pm 1$ while it remains localized on the orthogonal directions, which confirms the existence of such a mobile bound state.

For excitons separated by more than one site, the state evolution is governed by $\hat{H}_{\text{eff}}'$. Unlike spin systems reported earlier [23,46], the long-range interaction U_{ij} can be tuned much larger than the exchange rate J_{ij} here, which results in a highly anisotropic *XXZ* model and permits the existence of high-order bound states. If the NNN interaction $U_{i,i+2}$ is sufficiently larger than the NN hopping rate $J_{i,i+1}$, excitons separated by one lattice site also form bound states and exhibit correlated motion. Different from the dimer state $|\Psi_{i,i+1}\rangle$, transport of the high-order bound state $|\Psi_{i,i+2}\rangle$ relies on a second-order process with hopping rate $\sim J_{i,i+1}^2 / U_{i,i+2}$ [see the upper panel of Fig. 3(b)]. As verified by numerical results shown in Fig. 3(b), $g_{i,j}^{(2)}$ also localizes on the skew diagonals, but spreads on the

$j = i \pm 2$ diagonals in this case. The influence of dephasing on this highly nonlocal correlated behavior is also investigated. In Fig. 3(c), we calculate the correlation function for $t > 1/\gamma$, with γ the dephasing rate introduced previously. Interestingly, the strong bunching of $g_{i,j}^{(2)}$ along $i = j \pm 2$ survives, although its distribution is different from the coherent case. The small and uniform distribution of $g_{i,j}^{(2)}$ for $|i - j| > 2$ indicates the diffusion equilibrium for unpaired free excitons has been established, while the strong NN interaction $U_{i,i+1}$ forbids the diffusion into $|i - j| = 1$ region. To gain a deeper insight into such a correlated transport, we investigate the c.m. motion of two excitons. For coherent transport, this motion is characterized by a quantum random walk [49], with a density distribution described by the Bessel function [see the upper panel of Fig. 3(d)]. In contrast, the c.m. density distribution at $t > 1/\gamma$ is well fitted by a Gaussian function [see the lower panel of Fig. 3(d)]. This indicates that the high-order bound state we study exhibits diffusive expansion as a composite, which does not reach equilibrium due to its reduced diffusion rate compared to free excitons.

In conclusion, we propose a Rydberg-atom system for studying quantum transport dynamics, utilizing synthetic spin-exchange induced by vdW interaction. Our scheme does not require resonant DDI or off-diagonal vdW interaction, and thus avoids the complicated excitation schemes in multi-Rydberg-level systems. For the state-of-the-art experimental setup, its typical Rydberg lifetime ~ 50 μs [10] will not hinder the exciton transport we discuss, and its influence on the dynamics can be eliminated by using projective measurement [28]. In addition to simulating quantum transport phenomena, this work opens up an avenue towards constructing exotic spin models with Rydberg atoms, which, for instance, can facilitate the study of many-body localization [50,51].

---

[*]shuoyang@mail.tsinghua.edu.cn
[†]lyou@mail.tsinghua.edu.cn

[1] J. I. Cirac and P. Zoller, Nat. Phys. **8**, 264 (2012).
[2] I. M. Georgescu, S. Ashhab, and F. Nori, Rev. Mod. Phys. **86**, 153 (2014).
[3] D. S. Weiss and M. Saffman, Phys. Today **70**, No. 7, 44 (2017).
[4] M. Saffman, T. G. Walker, and K. Mølmer, Rev. Mod. Phys. **82**, 2313 (2010).
[5] H. Labuhn, D. Barredo, S. Ravets, S. De Léséleuc, T. Macrì, T. Lahaye, and A. Browaeys, Nature (London) **534**, 667 (2016).
[6] H. Bernien, S. Schwartz, A. Keesling, H. Levine, A. Omran, H. Pichler, S. Choi, A. S. Zibrov, M. Endres, M. Greiner et al., Nature (London) **551**, 579 (2017).
[7] M. Marcuzzi, J. Minář, D. Barredo, S. de Léséleuc, H. Labuhn, T. Lahaye, A. Browaeys, E. Levi, and I. Lesanovsky, Phys. Rev. Lett. **118**, 063606 (2017).
[8] H. Kim, Y. J. Park, K. Kim, H.-S. Sim, and J. Ahn, Phys. Rev. Lett. **120**, 180502 (2018).
[9] E. Guardado-Sanchez, P. T. Brown, D. Mitra, T. Devakul, D. A. Huse, P. Schauß, and W. S. Bakr, Phys. Rev. X **8**, 021069 (2018).
[10] H. Levine, A. Keesling, A. Omran, H. Bernien, S. Schwartz, A. S. Zibrov, M. Endres, M. Greiner, V. Vuletić, and M. D. Lukin, Phys. Rev. Lett. **121**, 123603 (2018).
[11] D. Barredo, V. Lienhard, S. De Leseleuc, T. Lahaye, and A. Browaeys, Nature (London) **561**, 79 (2018).
[12] N. Takei, C. Sommer, C. Genes, G. Pupillo, H. Goto, K. Koyasu, H. Chiba, M. Weidemüller, and K. Ohmori, Nat. Commun. **7**, 13449 (2016).
[13] I. Žutić, J. Fabian, and S. D. Sarma, Rev. Mod. Phys. **76**, 323 (2004).
[14] H. Najafov, B. Lee, Q. Zhou, L. C. Feldman, and V. Podzorov, Nat. Mater. **9**, 938 (2010).
[15] E. Collini, Chem. Soc. Rev. **42**, 4932 (2013).
[16] P. Jurcevic, B. P. Lanyon, P. Hauke, C. Hempel, P. Zoller, R. Blatt, and C. F. Roos, Nature (London) **511**, 202 (2014).
[17] G. M. Akselrod, P. B. Deotare, N. J. Thompson, J. Lee, W. A. Tisdale, M. A. Baldo, V. M. Menon, and V. Bulović, Nat. Commun. **5**, 3646 (2014).
[18] D. Barredo, H. Labuhn, S. Ravets, T. Lahaye, A. Browaeys, and C. S. Adams, Phys. Rev. Lett. **114**, 113002 (2015).
[19] D. W. Schönleber, A. Eisfeld, M. Genkin, S. Whitlock, and S. Wüster, Phys. Rev. Lett. **114**, 123005 (2015).
[20] A. P. Orioli, A. Signoles, H. Wildhagen, G. Günter, J. Berges, S. Whitlock, and M. Weidemüller, Phys. Rev. Lett. **120**, 063601 (2018).
[21] G. Günter, H. Schempp, M. Robert-de Saint-Vincent, V. Gavryusev, S. Helmrich, C. Hofmann, S. Whitlock, and M. Weidemüller, Science, **342**, 954 (2013).
[22] H. Schempp, G. Günter, S. Wüster, M. Weidemüller, and S. Whitlock, Phys. Rev. Lett. **115**, 093002 (2015).
[23] F. Letscher and D. Petrosyan, Phys. Rev. A **97**, 043415 (2018).
[24] S. Wüster, C. Ates, A. Eisfeld, and J. Rost, New J. Phys. **13**, 073044 (2011).
[25] A. W. Glaetzle, M. Dalmonte, R. Nath, C. Gross, I. Bloch, and P. Zoller, Phys. Rev. Lett. **114**, 173002 (2015).
[26] R. M. W. van Bijnen and T. Pohl, Phys. Rev. Lett. **114**, 243002 (2015).
[27] I. Shavitt and L. T. Redmon, J. Chem. Phys. **73**, 5711 (1980).
[28] See Supplemental Material at http://link.aps.org/supplemental/10.1103/PhysRevLett.123.063001 for details on derivations of the many-body effective Hamiltonian, exciton transport dynamics in a realistic system, and topological exciton pumping.

[29] M. Christandl, N. Datta, A. Ekert, and A. J. Landahl, Phys. Rev. Lett. **92,** 187902 (2004).

[30] W. K. Wootters, Phys. Rev. Lett. **80,** 2245 (1998).

[31] I. Lesanovsky and J. P. Garrahan, Phys. Rev. Lett. **111,** 215305 (2013).

[32] V. Lienhard, S. de Léséleuc, D. Barredo, T. Lahaye, A. Browaeys, M. Schuler, L.-P. Henry, and A. M. Läuchli, Phys. Rev. X **8,** 021070 (2018).

[33] H. Haken and P. Reineker, Z. Phys. **249,** 253 (1972).

[34] H. Haken and G. Strobl, Z. Phys. **262,** 135 (1973).

[35] P. Reineker, Phys. Lett. **42A,** 389 (1973).

[36] D. J. Thouless, Phys. Rev. B **27,** 6083 (1983).

[37] Y. Qian, M. Gong, and C. Zhang, Phys. Rev. A **84,** 013608 (2011).

[38] L. Wang, M. Troyer, and X. Dai, Phys. Rev. Lett. **111,** 026802 (2013).

[39] M. Lohse, C. Schweizer, O. Zilberberg, M. Aidelsburger, and I. Bloch, Nat. Phys. **12,** 350 (2016).

[40] S. Nakajima, T. Tomita, S. Taie, T. Ichinose, H. Ozawa, L. Wang, M. Troyer, and Y. Takahashi, Nat. Phys. **12,** 296 (2016).

[41] H.-I. Lu, M. Schemmer, L. M. Aycock, D. Genkina, S. Sugawa, and I. B. Spielman, Phys. Rev. Lett. **116,** 200402 (2016).

[42] E. J. Mueller, Phys. Rev. A **70,** 041603(R) (2004).

[43] M. J. Rice and E. J. Mele, Phys. Rev. Lett. **49,** 1455 (1982).

[44] Q. Niu and D. Thouless, J. Phys. A **17,** 2453 (1984).

[45] F. Mei, G. Chen, L. Tian, S.-L. Zhu, and S. Jia, Phys. Rev. A **98,** 032323 (2018).

[46] T. Fukuhara, P. Schauß, M. Endres, S. Hild, M. Cheneau, I. Bloch, and C. Gross, Nature (London) **502,** 76 (2013).

[47] P. M. Preiss, R. Ma, M. E. Tai, A. Lukin, M. Rispoli, P. Zupancic, Y. Lahini, R. Islam, and M. Greiner, Science **347,** 1229 (2015).

[48] T. Amthor, C. Giese, C. S. Hofmann, and M. Weidemüller, Phys. Rev. Lett. **104,** 013001 (2010).

[49] O. Mülken and A. Blumen, Phys. Rep. **502,** 37 (2011).

[50] P. Ponte, Z. Papić, F. Huveneers, and D. A. Abanin, Phys. Rev. Lett. **114,** 140401 (2015).

[51] J. Smith, A. Lee, P. Richerme, B. Neyenhuis, P. W. Hess, P. Hauke, M. Heyl, D. A. Huse, and C. Monroe, Nat. Phys. **12,** 907 (2016).